Journal of Materials Chemistry C

Accepted Manuscript

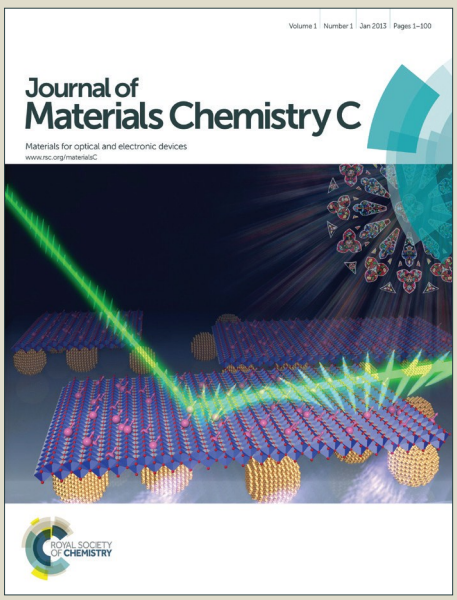

ROYAL SOCIETY OF CHEMISTRY

www.rsc.org/materialsC

Journal of Materials Chemistry C

ARTICLE

Graphene nanosheets/$BaTiO_3$ ceramics as highly efficient electromagnetic interference shielding materials in the X–band

Received 00th January 20xx,
Accepted 00th January 20xx

DOI: 10.1039/x0xx00000x

www.rsc.org/MaterialsC

Qing Yuchang*, Wen Qinlong, Luo Fa, Zhou Wancheng, Zhu Dongmei

Graphene nanosheets (GNs) filled $BaTiO_3$ ceramics with high-performance electromagnetic interference (EMI) shielding were prepared via pressureless sintering. Both of the real and imaginary part of complex permittivity increased with increasing GN content. The EMI shielding results showed that absorption mechanism is the main contribution to the total EMI shielding effectiveness (SE). The total EMI SE is greater than 40 dB in the X–band at 1.5 mm thickness, which suggests the GNs-$BaTiO_3$ ceramics could be good candidates for highly efficient EMI shielding material in the whole X–band.

1. Introduction

The electromagnetic (EM) pollution, raised by the extensive development of telecommunication devices and GHz electronic systems, has quest for novel and effective EM interference (EMI) shielding material. The shielding effectiveness (SE) can be achieved by minimizing the signal passing through a material filled with conductive, dielectric and/or magnetic absorbers. [1–10] The shielding performance in the frequency range of 8.2−12.4 GHz (X−band) is important due to the EMI shielding material is widely used in X–band for military and communication applications, such as radar, telephone microwaves, and TV picture transmission. Great efforts have been made for development of high-performance EMI shielding materials. [11–15] It is also well known that the content, dispersion, intrinsic conductivity and dielectric properties of the filler contribute to the total EMI SE of a filler filled composite. Conductive particles, especially carbon nanotubes (CNTs), graphene nanosheets (GNs) and graphene (GP), with high electrical conductivity were used to minimize various microwave radiations and interferences owing to their unique morphology, relatively low density and mixing ratios, and excellent electrical properties. [16–37]

Among these carbon nano-materials, the unique properties of GP and GNs have attracted much attention as very promising and lightweight absorber to fabricate EMI shielding composites over the past decade. [19–37] The EMI SE of 15 wt% GP filled epoxy resin can be obtained with 21 dB over X–band. [19] GP/poly(dimethyl siloxane) foam composite with ~0.8 wt% GP shows an EMI SE of ~20 dB in the X–band at ~1 mm thickness. [20] The EMI SE of the reduced graphene oxide (rGO) /PS composites exhibit higher EMI SE of 45.1 dB at 2.5 mm thicknesses while 22.2 dB at 1.5 mm. [21] The obtained porous 30 wt% functionalized GP sheets filled PS composite achieved an EMI SE of approximately 29 dB at 2.5 mm thickness. [22] A high EMI SE of ~30 dB was obtained for the 8 wt% GP filled PMMA composite at ~3.4 mm thickness. [26] These experimental results show that GP and GNs with unique properties could be very promising and lightweight absorber for designing EMI shielding material.

Despite the success of several studies in development of GP/polymer composites with high EMI SE at specific frequencies, there are still seldom reports about GNs filled ceramics and then investigated the complex permittivity and EMI properties of such composites. Recently, the EMI SE of the graphitized reduced graphene oxides (r-GOs)/SiO_2 composites with 20 wt% r-GOs reaches a maximum at 35 dB at ~ 1.5 mm thickness. However, these r-GOs/SiO_2 composites also suffer from the poor electrical conductivity under lower content of r-GOs, which contributed to the EMI shielding performance should be not high. For example, the EMI SE can reach to only 12 dB when such composites filled with 8 wt% r-GOs. [28] Thus, the fabrication of GP filled ceramics with a high EMI SE under low GP content remains a daunting challenge. In addition, CNTs/$BaTiO_3$ ceramics with high electrical conductivity also have been studied [38], which also indicated that the $BaTiO_3$ ceramic filled with GNs can be used as EMI shielding materials with excellent microwave attenuation property.

In this work, low GN content filled $BaTiO_3$ ceramics with high–performance EMI SE were prepared via pressureless sintering. The microstructure, complex permittivity and EMI SE of the GNs-$BaTiO_3$ ceramics in the X-band, as well as the effects of GN contents on the EMI shielding mechanism (absorption and reflection) of the total EMI SE (SE_{Total}), were measured and analyzed. The obtained GNs filled $BaTiO_3$ ceramic, with a thickness of only 1.5 mm and content of 4 wt% GNs, exhibits an average EMI SE of 41.7 dB in the X–band, which showed excellent EMI SE for GNs filled $BaTiO_3$ ceramic at such a low GNs content and ceramic thickness.

State Key Laboratory of Solidification Processing, School of Materials Science and Engineering, Northwestern Polytechnical University, Xi'an 710072, China. Fax: +86 29 8849 4574. E-mail: qtvbgyta@163.com

2. Materials and methods

The GNs were obtained by exfoliation of graphite with typical thickness and lateral dimensions of about 1–5 nm and 5–15 μm, respectively. Tetragonal-phase $BaTiO_3$ powder with a Ba/Ti mol ratio of 1.001, were provided by Nantong Ao Xin Electronic Technology Co. Ltd., JiangSu, China. The D50 of the $BaTiO_3$ powder is about 500 nm. The content of GNs was 0, 1, 2, 3, and 4 wt% and the corresponding samples were designated as GN0, GN1, GN2, GN3, and GN4 for simplicity. The starting mixture was mixed for 12 h using ethyl alcohol and ZrO_2 balls. Then the powders were dried by rotary evaporation and sieved through a 400–mesh screen. Rectangle pellets were shaped by uniaxial pressing at 50 MPa, followed by cold isostatic pressing at 200 MPa for 2 min. Sintering was carried out in a high temperature graphite resistant furnace at temperature 1300 °C for 2 h under argon atmosphere. In order to determined the effect of $BaTiO_3$ matrix on the EMI properties, the values of the complex permittivity and EMI SE of the 4 wt% GN filled epoxy (designated as GN-P) were also prepared and measured.

Transmission electron microscope (TEM) observation was performed using a JEM-2100 microscope (JEOL, Limited, Tokyo, Japan) operating at an accelerating voltage of 200 kV. Field emission scanning electron microscopy (FE-SEM), X-ray Diffraction (XRD) and Raman analysis was used to analyze the characterization of GNs filled $BaTiO_3$ ceramics. Atom force microscopy (AFM) was performed using a Nanoscope-IIIa scanning probe microscope in the taping mode. The sample for AFM observation was prepared by spin coating the ethyl alcohol dispersion of the GNs onto a pre-cleaned silicon wafer. The electrical conductivity was measured by two-wire method using a current source Keithley 6220 DC. The testing specimens for the EM properties measurement were cut into rectangular blocks with dimensions of 22.86 mm (length) × 10.16 mm (width) × 1.5 mm (thickness). The transmission and reflection scattering parameters (S_{11}/S_{22} and S_{21}/S_{12}), the complex permittivity ($\varepsilon=\varepsilon'-j\varepsilon''$) of the ceramics were measured by Agilent technologies E8362B network analyzer in the frequency range of 8.2-12.4 GHz using wave-guide method, which was based on the measurements of the reflection and transmission module and in the fundamental wave–guide mode TE_{10}. From S_{11} (S_{22}) and S_{21} (S_{12}) measurements, reflected coefficient (R) and transmitted coefficient (T) is given by: $R = |E_R/E_I|^2 = |S_{11}|^2 = |S_{22}|^2$ and $T = |E_T/E_I|^2 = |S_{21}|^2 = |S_{12}|^2$. The absorbed coefficient (A) can be obtained by A=1−R−T. The total EMI SE of a material and the contribution of absorption (SE_A) and reflection (SE_R) to the total EMI SE were also calculated from the S parameters by the following equations: [39]

$$\text{Total EMI SE} = SE_R + SE_A = 10\log\frac{1}{|S_{21}|^2} \quad (1)$$

$$SE_R = 10\log\frac{1}{1-|S_{11}|^2} \quad (2)$$

$$SE_A = 10\log\frac{1-|S_{11}|^2}{|S_{21}|^2} \quad (3)$$

3. Results and discussions

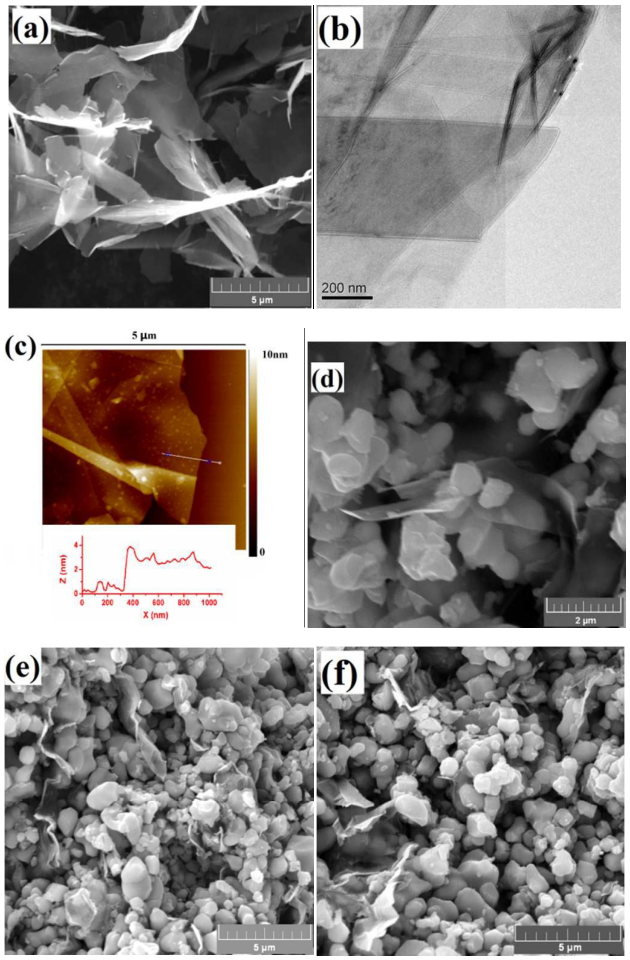

Fig. 1 (a) SEM and (b) TEM images of the GNs. (c) AFM images of GNs on silicon. Typical SEM images of the (d) GNs-$BaTiO_3$ starting mixture and (e, f) fracture surface of sintered GNs-$BaTiO_3$ ceramics.

It is clear that GNs exhibited unique two dimensional plates with a smooth and mat-like structure, as showed in Fig.1a and b. The AFM (Fig. 1c) shows GNs with typical thickness of about 4 nm.Fig.1 also shows the typical FE-SEM images of GNs-$BaTiO_3$ ceramic filled with 4 wt% GNs (d) before and (e, f) after sintering. The SEM images clearly indicate the GNs-$BaTiO_3$ ceramics prepared by pressureless sintering are not dense with the porosity is about 8~10 %. Furthermore, the GNs were individually distributed throughout the $BaTiO_3$ matrix and that no GN aggregations were found. Homogeneous dispersion of the GNs throughout the $BaTiO_3$ matrix and GNs with a large platelet also protrude out of the fracture surface the $BaTiO_3$ matrix, as show in Fig. 1 e and f.

The XRD patterns of the GNs-$BaTiO_3$ ceramics with different GN content are show in Fig. 2a. A new peak at 2θ angles of about 26.3°, corresponds to crystalline carbon, is observed as GNs added into the $BaTiO_3$ ceramics. Although the $BaTiO_3$ crystallize is still in the perovskite structure, the phase of $BaTiO_3$ change from cubic to tetragonal phase after sintering is evidenced. There is no detectable second phase indicating that there has not been any significant reaction between the GNs and crystalline $BaTiO_3$ particles. Fig. 2b shows Raman spectra of the GNs powders and GNs-$BaTiO_3$ ceramics in the

1000–3000 cm^{-1} region. The Raman patterns of GNs show a strong G peak at around 1580 cm^{-1}, a disorder-induced band around 1350 cm^{-1} (D), and 2D peak around 2700 cm^{-1}. After 1300 °C sintering, the intensity of the D band, characteristic of disorder, decreased while the G band, assigned to a graphitic structure, increased. The I_D/I_G ratio is about 0.396 for GNs, and it decreases to 0.293 after sintering in 1300 °C. The Raman spectra also indicated that a more ordered GNs after sintering can be obtained due to the amorphous carbon on the surface of GNs is removed and honeycomb hexagonal lattice is recovered to some extent. [25]

Fig.3. shows the real (ε′) and imaginary (ε″) part of complex permittivity of the GNs-$BaTiO_3$ ceramics and GNs filled epoxy. The value of ε′ and ε″ of the 4 wt% GNs filled epoxy is about 12.4 and 2.0 at the frequency of 8.2 GHz, respectively. Both the values of ε′ and ε″ of the GNs-$BaTiO_3$ ceramics increased with increasing GN content in the whole measured frequency region. For example, the highest values of ε′ and ε″ of the ceramic contain 4 wt% GNs can be reached to 123.8 and 136.1 at the frequency of 8.2 GHz, respectively, which ε′ is about 10 times and ε″ is almost 68 times larger than that of the GNs filled epoxy with the same GN content at 8.2 GHz. It is well known that the complex permittivity of the $BaTiO_3$ is larger than that of the epoxy, therefore, higher complex permittivity can be obtained when $BaTiO_3$ was used as matrix. Thus, compared with the polymer filled with GNs, high dielectric constant $BaTiO_3$ matrix also have significant influence on the complex permittivity of such ceramics, which also increased the total EMI SE of the GNs-$BaTiO_3$ ceramics. Obviously, the GNs are included into the $BaTiO_3$ matrix to constitute heterogeneous composites. More relaxation polarization is introduced as the GN content increased. From this point of view, the higher value of ε′ can be obtained with the higher GN content.

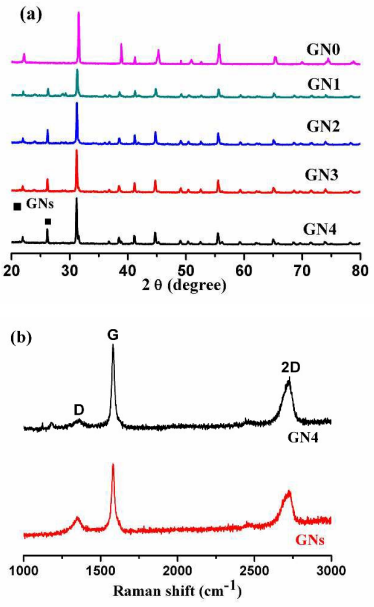

Figure 2. (a) XRD and (b) Raman of the GNs-$BaTiO_3$ ceramics.

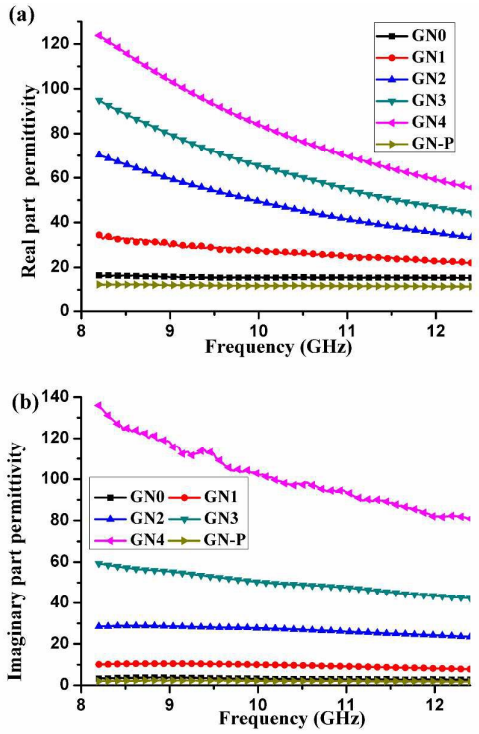

Fig.3. The (a) real and (b) imaginary part of complex permittivity of GNs-BaTiO3 ceramics with different GN content and GNs filled epoxy.

The value of ε" of the GNs-$BaTiO_3$ ceramics is mainly depended on two different factors in the microwave frequency range: relaxation phenomenon and electrical conductivity, it can be expressed by the equation: $\varepsilon = \varepsilon''_{\mathrm{relax}} + \sigma/\omega\varepsilon_0$, where ε''_{relax} is electron relaxation polarization in this case, σ is the electrical conductivity, ε_0 is the dielectric constant in vacuum, and ω is the angular frequency. [40] According to this equation, both the ε''_{relax} and σ will be enhanced when the GN content increased, and resulting in the enhancement of the value of ε″. Furthermore, the ceramics with higher GN content have higher number of interfacial electric dipolar polarization and require larger relaxation time at tested frequency range. Therefore, higher values and frequency dependence of ε′ and ε″ can be obtained under the higher electrical conductivity of such ceramics, as showed in the Fig. 3. Compared with other carbon nano-materials filled ceramics, the high value of ε′ and ε″ for such ceramics is reasonable due to the flaky GNs, as showed in Fig. 1. The microstructure of flaky GNs in such ceramics affects the formation of microcapacitor network and the evolution of conductive path, and then influences both the vaules and frequency dependence of ε′ and ε″. Additionally, the ε′ and ε″ of GNs-$BaTiO_3$ ceramics can be further enhanced if the porosity of such ceramics decreased, such as using hot pressed or spark plasma sintering process. The average values of loss tangent of such ceramics increased from 0.35 to 1.25 as the GN content increased from 1 to 4 wt%, which suggesting the GNs-$BaTiO_3$ ceramics with high complex permittivity and dielectric loss could be good candidates for the EMI shielding materials in the measured frequency region.

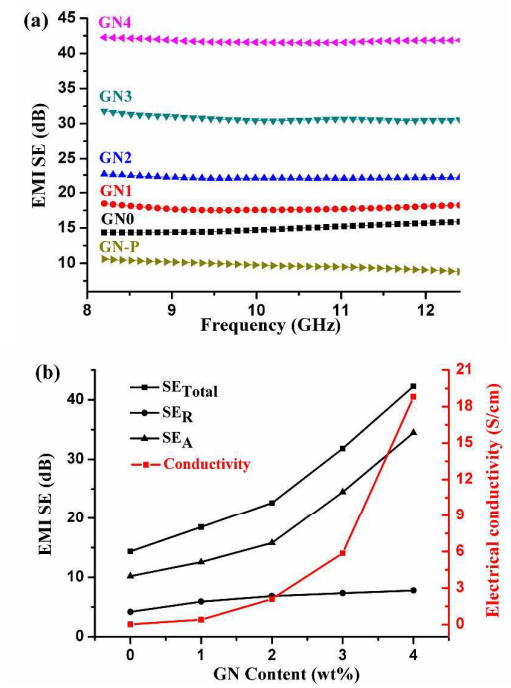

Fig. 4. (a) EMI SE of GNs-$BaTiO_3$ ceramics with different GN content and GNs filled epoxy in the X-band at 1.5mm thickness. (b) EMI SE, SE_R and SE_A at the frequency of 8.2 GHz and electrical conductivity of GNs-$BaTiO_3$ ceramics as a function of GN content.

Fig.4a shows the EMI SE of the GNs-$BaTiO_3$ ceramics and GNs filled epoxy as a function of GN content in the X-band and at 1.5 mm thickness. It is obvious to conclude that the values of EMI SE increased in the whole measured frequency range as the GN content increased. It is also evident that the main contribution to the EMI shielding comes from the addition of the GNs. An EMI SE value of at least 20 dB is typically required for commercially application in EMI shielding devices. [22] The values of the EMI SE were about 22 dB in the whole X-band at lower content of GNs with 2 wt%. The highest EMI SE was observed for such ceramic filled with 4 wt% GNs, and the value of EMI SE greater than 40 dB and is about 4 times larger than that of the 4 wt% GNs filled epoxy, denoting high dielectric constant $BaTiO_3$ matrix also have significant influence on the EMI properties and resulted excellent EMI shielding properties in the whole X-band.

The enhancement mechanism of EMI SE of the GNs-$BaTiO_3$ ceramics could be interpreted in three ways: the first was concerned with the excellent dispersion of the GNs in the $BaTiO_3$ ceramic, as evident from the Fig.1. An excellent dispersion of GNs in the $BaTiO_3$ matrix ensures excellent conductivity and EM absorber throughout the whole ceramics, which is also important for effective EMI shielding action. The second was the structure and high conductivity properties of GNs were retained after sintering which ensured the high EMI SE of such ceramics. Moreover, compared with the GNs filled polymer composites, high dielectric constant $BaTiO_3$ powder also have significant influence on the complex permittivity of such composites, which also increased the EMI SE of the GNs-$BaTiO_3$ ceramics.

Table 1 Comparison of EMI SE of different GP-based composites in the X-band

Matrix	Absorber and Content	Thickness (mm)	EMI SE (dB)	Ref.
$BaTiO_3$	4.0 wt% GNs	1.5	41.7	This work
Epoxy	15wt% GP	2.0	21.0	[20]
PDMS foam	~0.8wt% GP	~ 1	20.0	[21]
PS	7.0 wt% rGO	2.5	45.1	[22]
PS foam	30.0 wt% GP	2.5	~29.0	[23]
WPU	~7.7wt% rGO	2.0	~32.0	[24]
WPU	7.5wt% rGO	2.0	~34.0	[25]
PMMA	~8.0wt%GP	~3.4	~30.0	[26]
PMMA foam	~5.0wt% GP	2.4	~19.0	[27]
SiO_2	20.0wt% rGO	~ 1.5	~35.0	[28]
Polyurethane	10 wt% MWCNT	1.5	~29.0	[29]

Therefore, the enhancement of the EMI SE of the GNs-$BaTiO_3$ ceramics was mainly contributed to the excellent dispersion of GNs in the $BaTiO_3$ matrix, the retained of GNs and the combination the advantages of GNs and $BaTiO_3$ ceramics. A detailed EMI SE property of the GNs-$BaTiO_3$ ceramics and comparison of other representative GP composites are summarized in the Table 1. These results indicate that the EMI SE of the GNs-$BaTiO_3$ ceramics in current work has been greatly improved at similar or even lower sample thicknesses and/or GP loadings, as listed in Table 1. Furthermore, compared with the GP filled polymer composites, GNs-$BaTiO_3$ ceramics, with low GN content and high EMI SE in the X-band, also exhibit a promising prospect for high temperature (up to 500 °C) applications.

The total EMI SE of GNs-$BaTiO_3$ ceramics was also divided into the reflection (SE_R) and absorption (SE_A) components. As evident from Fig. 4 b, the primary contribution to the SE_{Total} is absorption rather than reflection in the studied GNs content and frequency range. For example, for the ceramic filled with 4 wt% GNs, the SE_{Total} is about 42.3 dB, while the SE_A is about 34.5 dB and SE_R is about 7.8 dB. It is also obvious that both the SE_R and SE_A increased with increasing GN content. Moreover, it was found that SE_A increased much faster compared with SE_R as the GN content increased. Fig.4 b also shows the values of EMI SE at the frequency of 8.2 GHz and electrical conductivity as a function of GN content. As shown in Fig.4 b, the electrical conductivity of the ceramics increased with increasing GN content, especially when the GN content reach to 3 wt%. The increase of electrical conductivity is mainly attributed to higher intrinsic conductivity of GNs as well as increasing GN conductive network. The values of EMI SE of the GNs-$BaTiO_3$ ceramics increased from 18.5 to 42.3 dB at the frequency of 8.2 GHz when the GN content increased from 1 to 4 wt%. Obviously, the GNs-$BaTiO_3$ ceramics with higher GN content exhibited higher conductivity and greater EMI SE. Furthermore, the EMI SE of the GNs-$BaTiO_3$ ceramics can be further enhanced using hot pressed or spark plasma sintering process. Here, the prepared GNs-$BaTiO_3$ ceramics exhibited excellent EMI shielding performance, suggesting such ceramics serves as ultimate and promising choice for the future EM shielding materials with highly effective and broad bandwidth.

4. Conclusions

GNs-$BaTiO_3$ ceramics with excellent EMI SE were prepared by pressureless sintering method. The values of ε′, ε″, EMI SE, SE_R and SE_A of such ceramics were enhanced with increasing GN content in the whole X-band. Moreover, it was also found that SE_A increased much faster than SE_R, and the absorption is the major shielding mechanism of GNs-$BaTiO_3$ ceramics. The total EMI SE of 4 wt% GNs filled $BaTiO_3$ ceramic exceed 40 dB in whole X-band with a thickness of 1.5 mm, denoting such ceramic have excellent EM attenuation properties and can be used as commercially and effective shielding materials for EM applications.

Acknowledgements

This work was financially supported by National Natural Science Foundation of China (No. 51402239), State Key Laboratory of Solidification Processing (NWPU), China (Grant No. KP201422) and Fundamental Research Funds for the Central Universities (No. 3102014JCY01002).

Notes and references

1 N. Yousefi , X. Sun, X. Lin, X. Shen, J. Jia, B. Zhang, et. al. *Adv. Mater.*, 2014, **26**, 5480.
2 F. He, S. Lau, H.L. Chan and J. Fan. *Adv. Mater.*, 2009, **21**, 710.
3 M.S. Cao, X.X. Wang, W.Q. Cao and J. Yuan. *J. Mater. Chem. C*, 2015, **3**, 6589.
4 A.P. Singh, P. Garg, F. Alam, K. Singh, R.B. Mathur, R.P. Tandon, et. al. *Carbon*, 2012, **50**, 3868.
5 D.D.L. Chung, *Carbon*, 2001, **39**, 279.
6 Y. Chen, Y.L. Wang, H.B. Zhang, X.F. Li, C.X. Gui and Z.Z. Yu. *Carbon*, 2015, **82**, 67.
7 Y.C. Qing, D.D. Min, Y.Y. Zhou, F. Luo and W.C. Zhou, *Carbon*, 2015, **86**, 98.
8 M. Verma, A.P. Singh, P. Sambyal, B.P. Singh, S.K. Dhawan and V. Choudhary. *Phys. Chem. Chem. Phys.*, 2015, **17**, 1610.
9 M. Arjmand, M. Mahmoodi, G.A. Gelves, S. Park, U. Sundararaj, *Carbon*, 2011, **49**, 3430.
10 M.S. Cao, W.L. Song, Z.L. Hou, B. Wen and J. Yuan, *Carbon*, 2010, **48**, 788.
11 B. Wen, M.S. Cao, Z.L. Hou, W.L. Song, L. Zhang, M.M. Lu, et. al., *Carbon*, 2013, **65**, 124.
12 A.A. Khurram, S.A. Rakha, P. Zhou, M. Shafi, and A. Munir. *J. Appl. Phys.*, 2015, **118**, 044105.
13 T.K. Gupta, B.P. Singh, V.N. Singh, S. Teotia, A.P. Singh, I. Elizabeth, et. al., *J. Mater. Chem. A*, 2014, **2**, 4256.
14 H.D. Huang, C.Y. Liu, D. Zhou, X.Jiang, G.J. Zhong, D.X. Yan, et. al. *J. Mater. Chem. A*, 2015, **3**, 4983.
15 M. Mishra, A.P. Singh, B.P. Singh, V.N. Singh and S.K. Dhawan. *J. Mater. Chem. A*, 2014, **2**, 13159.
16 S.P. Pawar, D.A. Marathe, K. Pattabhi and S. Bose. *J. Mater. Chem. A*, 2015, **3**, 656.
17 A.P. Singh, M. Mishra, P. Sambyal, B. K.Gupta, B.P. Singh, A. Chandrad, et. al. *J. Mater. Chem. A*, 2014, **2**, 3581.
18 P. Saini and M. Arora. *J. Mater. Chem. A*, 2013, **1**, 8926.
19 W.L. Song, M.S. Cao, M.M. Lu, J. Liu, J. Yuan and L.Z. Fan. *J. Mater. Chem. C*, 2013, **1**, 1846.
20 J.J. Liang, Y. Wang, Y. Huang, Y.F. Ma, Z.F. Liu, J.M. Cai, et. al. *Carbon*, 2009, **47**, 922.
21 Z.P. Chen, C. Xu, C.Q. Ma, W.C. Ren and H.M. Cheng. *Adv. Mater*. 2013, **25**, 1296.
22 D.X. Yan, H. Pang, B. Li, R. Vajtai, L. Xu, P.G. Ren, et. al. *Adv. Funct. Mater.*, 2015, **25**, 559.
23 D.X. Yan, P.G. Ren, H. Pang, Q. Fu, M.B. Yang and Z.M. Li. *J. Mater. Chem.*, 2012, **22**, 18772.
24 S.T. Hsiao, C.C.M. Ma, H.W. Tien, W.H. Liao, Y.S. Wang, S.M. Li, et. al. *Carbon*, 2013, **60**, 57.
25 S.T. Hsiao, C.C.M. Ma, W.H. Liao, Y.S. Wang, S.M. Li, Y.C. Huang, et. al. *ACS Appl. Mater. Interfaces*, 2014, **6**, 10667.
26 H.B. Zhang, W.G. Zheng, Q. Yan, Z.G. Jiang and Z.Z. Yu. *Carbon*, 2012, **50**, 5117.
27 H.B. Zhang, Q. Yan, W.G. Zheng, Z.X. He and Z.Z. Yu. *ACS Appl. Mater. Interfaces*, 2011, **3**, 918.
28 B. Wen, M.S. Cao, M.M. Lu, W.Q. Cao, H.L. Shi, J. Liu, et. al. *Adv. Mater.*, 2014, **26**, 3484.
29 T.K. Gupta, B.P. Singh, S.R. Dhakate, V.N. Singh and R.B. Mathur. *J. Mater. Chem. A*, 2013, **1**, 9138.
30 G.P. Kar, S. Biswas, R. Rohini and S. Bose. *J. Mater. Chem. A*, 2015, **3**, 79.
31 A. P. Singh, M. Mishra, P. Sambyal, B. K. Gupta, B. P. Singh, A. Chandra and S. K. Dhawan, *J. Mater. Chem. A*, 2014, **2**, 3581.
32 W.L. Song, J. Wang, L.Z. Fan, Y. Li, C.Y. Wang and M.S. Cao, *ACS Appl. Mater. Interfaces*, 2014, **6**, 10516.
33 H. J. Yang, W. Q. Cao, D. Q. Zhang, T. J. Su, H. L. Shi, W. Z. Wang, J. Yuan and M. S. Cao, *ACS Appl. Mater. Interfaces*, 2015, **7**, 7073.
34 B. Wen, X. X. Wang, W. Q. Cao, H. L. Shi, M. M. Lu, G. Wang, H. B. Jin, W. Z. Wang, J. Yuan and M. S. Cao, *Nanoscale*, 2014, **6**, 5754.
35 J. Liu, W. Q. Cao, H. B. Jin, J. Yuan, D. Q. Zhang and M. S. Cao, *J. Mater. Chem. C*, 2015, **3**, 4670.
36 T. K. Gupta, B. P. Singh, V. N. Singh, S. Teotia, A. P. Singh, I. Elizabeth, S. R. Dhakate, S. K. Dhawan and R. B. Mathur, *J. Mater. Chem. A*, 2014, **2**, 4256.
37 T. K. Gupta, B. P. Singh, R. B. Mathur and S. R. Dhakate, *Nanoscale*, 2014, **6**, 842.
38 Q. Huang and L. Gao. *J. Mater. Chem.*, 2004, **14**, 2536.
39 Y.C. Qing, Y. Mu, Y.Y. Zhou, F. Luo, D.M. Zhu and W.C. Zhou. *J. Europ. Ceram. Soc.*, 2014, **34**, 2229.
40 Y.C. Qing, W.C. Zhou, S. Jia, F. Luo and D.M. Zhu, *Appl. Phys. A*, 2010, **100**, 1177.